Nuclear Engineering and Technology 51 (2019) 1991–1997

Contents lists available at ScienceDirect

Nuclear Engineering and Technology

journal homepage: www.elsevier.com/locate/net

Original Article

Ambient dose equivalent measurement with a CsI(Tl) based electronic personal dosimeter

Kyeongjin Park [a], Jinhwan Kim [a], Kyung Taek Lim [a], Junhyeok Kim [a], Hojong Chang [b], Hyunduk Kim [c], Manish Sharma [d], Gyuseong Cho [a, *]

[a] Department of Nuclear and Quantum Engineering, Korea Advanced Institute of Science and Technology, 291 Daehak-ro, Yuseong-gu, Daejeon, 34141, Republic of Korea
[b] Institute for Information Technology Convergence, Korea Advanced Institute of Science and Technology, 291 Daehak-ro, Yuseong-gu, Daejeon, 34141, Republic of Korea
[c] IRIS Co., Ltd., 193, Munji-ro, Yuseong-gu, Daejeon, 34051, Republic of Korea
[d] Department of Nuclear Engineering, Khalifa University, Abu Dhabi, 127788, United Arab Emirates

ARTICLE INFO

Article history:
Received 14 February 2019
Received in revised form
6 June 2019
Accepted 17 June 2019
Available online 18 June 2019

Keywords:
Electronic personal dosimeter
Ambient dose equivalent
$G(E)$ function
PIN diode
CsI(Tl) scintillator

ABSTRACT

In this manuscript, we present a method for the direct calculation of an ambient dose equivalent ($H^*(10)$) for the external gamma-ray exposure with an energy range of 40 keV to 2 MeV in an electronic personal dosimeter (EPD). The designed EPD consists of a 3 × 3 mm^2 PIN diode coupled to a 3 × 3 × 3 mm^3 CsI (Tl) scintillator block. The spectrum-to-dose conversion function ($G(E)$) for estimating $H^*(10)$ was calculated by applying the gradient-descent method based on the Monte-Carlo simulation. The optimal parameters for the G(E) were found and this conversion of the $H^*(10)$ from the gamma spectra was verified by using ^{241}Am, ^{137}Cs, ^{22}Na, ^{54}Mn, and ^{60}Co radioisotopes. Furthermore, gamma spectra and $H^*(10)$ were obtained for an arbitrarily mixed multiple isotope case through Monte-Carlo simulation in order to expand the verification to more general cases. The $H^*(10)$ based on the $G(E)$ function for the gamma spectra was then compared with $H^*(10)$ calculated by simulation. The relative difference of $H^*(10)$ from various single-source spectra was in the range of ±2.89%, and the relative difference of $H^*(10)$ for a multiple isotope case was in the range of ±5.56%.

1. Introduction

Since the time that radiation was introduced to modern medicine, nondestructive testing (NDT), and material-process industries (including nuclear power plants), some specific quantities such as the air exposure, the air kerma, and equivalent or effective doses have been used in order to evaluate the risk of health effects on radiation workers and the public. The International Commission on Radiological Units and Measurements (ICRU) has defined measureable quantities that provide convenient and appropriate evaluations for area and personal radiation monitoring as well as dosimetry [1]. In particular, for photons (gamma-rays and X-rays) and neutrons above the energy of 15 keV, an appropriate quantity for monitoring a specific area was defined as the ambient dose equivalent $H^*(10)$. The definition of $H^*(10)$ is the dose equivalent that would be produced by a corresponding expanded and aligned field at a depth of 10 mm in the ICRU sphere on the radius opposing the direction of the aligned field [1]. However, despite its simple definition, the practical measurements by using any radiation detector are not trivial because the precise conversion from the measured signal to $H^*(10)$ value is difficult for many reasons. GM counters and plastic scintillation detectors are the most inexpensive and widely used radiation detectors, but they are subject to some limitations to be used as dosimeters.

Firstly, the most simple but most popular radiation detector is the Geiger-Muller (GM) counter. However, the GM counter cannot provide spectral data, but only provides counts or count rates. Therefore, in order to use the GM counter as a dosimeter, a typically specific design of a GM counter wall is necessary to guarantee that the count is proportional to the final target quantity such as the air exposure or $H^*(10)$. This method is imperfect because of the nonlinearity of the count-to-dose conversion over a wide gamma-ray energy range. In practice, GM-based dosimeters are used with a periodic calibration process at only 662 keV emitted from a

* Corresponding author.
E-mail addresses: gscho@kaist.ac.kr, gscho1@kaist.ac.kr (G. Cho).

https://doi.org/10.1016/j.net.2019.06.017

standard ^{137}Cs source worldwide. Secondly, one kind of ideal detector for gamma-ray absorbed dose measurements is a plastic scintillation detector. This is because plastic is a tissue equivalent material in its atomic composition. Therefore, in a sense, the light yield of the plastic scintillator is proportional to $H^*(10)$, but the plastic scintillator requires a large volume at low dose rates or at high energies due to its extremely low interaction efficiency [2]. Furthermore, it is very difficult to identify the types of radioisotopes from the gamma spectra from typical plastic scintillators since there are no prominent photo-peaks for gamma rays. Other types of radiation detectors, such as gas ionization chambers and proportional counters, inorganic scintillation detectors, and semiconductor detectors, can provide a gamma-ray spectrum with photo-peaks, which can be used to identify the gamma-ray sources, i.e. isotope types. The energy spectra of these detectors can be used to estimate dosimetric quantities such as the air exposure, the air kerma, $H^*(10)$, and activities of individual gamma sources through a conversion process. Several studies have shown that $H^*(10)$ can be obtained using inorganic scintillators such as NaI(Tl), CsI(Tl), LaBr3(Ce), and semiconductor detectors from the gamma-ray spectra [2–6].

There are two methods for estimating $H^*(10)$ from the gamma-ray spectra. The first method is a two-step process. The first step is to deduce the fluence spectrum of the gamma-rays incident onto the detector from the measured gamma-ray spectrum of a particular detector in use. This fluence spectrum could be a sum of individual gamma-rays energy spectra. This is typically done by stripping or unfolding the measured spectrum using a detector response matrix, which is calculated by Monte-Carlo simulations with an assumed geometry and detector information such as shape, size, and material composition [2–5]. As a second step, $H^*(10)$ can be calculated via the gamma-ray fluence-to-$H^*(10)$ conversion factors, $C(E)$, provided by ICRP 74 publication [7].

The second method is to use the spectrum-to-dose conversion function, $G(E)$, directly. This method has been used to obtain the air exposure, the air kerma, or the ambient dose rates, $H^*(10)$, etc. directly from the measured spectra [8–13]. The $G(E)$ function is typically described by a polynomial function that has the power of the natural logarithm of the energy, and their coefficients can be calculated by the least-squares method (LSM) when the measured spectra and $H^*(10)$ values of a number of gamma-ray sources are available. These $H^*(10)$ values can be calculated with the $C(E)$ function for the sources of known activities at a specific distance or can be measured by other calibrated dosimeters.

In this work, we propose an electronic personal dosimeter (EPD) for gamma-ray detection, of which the main body is operated by a mobile app via Bluetooth communication. The gamma-ray sensor is a 3 × 3 × 3 mm^3 CsI(Tl) scintillation detector glued onto a 3 × 3 mm^2 PIN diode chip. The proposed EPD system can directly measure $H^*(10)$ in real time using the $G(E)$ function. The $G(E)$ function of the sensor was obtained by the gradient-descent method (GDM), which is one of the neural network techniques. As input variables, the gamma spectra and $H^*(10)$ values were provided by using Monte-Carlo simulation (MCNP6) [14]. The validity of the Monte-Carlo simulation results was verified by comparing with the measurements of spectra from five isotopes. Finally, the relative differences of the $H^*(10)$ values obtained by the $G(E)$ function method and the MCNP6 option for $H^*(10)$ were estimated for the same simulation condition.

2. Materials and method

2.1. EPD hardware

A schematic of the main body of the proposed EPD system is shown in Fig. 1. The main body of the EPD consists of a sensor module (a 3 × 3 × 3 mm^3 CsI(Tl) scintillator cubical block coupled onto a 3 × 3 mm^2 PIN diode chip), a signal processing board (a preamplifier, a shaping amplifier, a sample and hold circuit, and a micro control unit (MCU) with a Bluetooth module) and a power supply circuitry.

The most widely used radiation detector is the scintillation detector, e.g., a scintillator combined with a photodetector. Conventionally, vacuum photomultiplier tubes (PMTs) are the popular choice for photodetectors in a scintillation detector due to their high quantum efficiency in 400 nm range, high gain, high single photon sensitivity, fast response, and low noise. However, their bulky size and high operation voltage (1000–3000 V) became limiting factors when it came down to constructing a portable radiation-monitoring device, for example, an EPD. Thus, because of these disadvantages of PMTs, silicon photomultipliers (SiPMs) have been considered as an alternative solution in replacing traditional PMTs due to their comparable high gain, good detection efficiency, fast response, compactness, and low operation bias (24–70 V) [15–17]. Nonetheless, relatively high dark currents generated from most of current the SiPMs are even more challenging to integrate SiPMs for EPDs in terms of power management. The size of a power supply required to operate SiPMs for a few days or so is still large and bulky, especially for EPDs. On the other hand, the silicon-based PIN diode has been a widely used solid-state photodetector for the scintillation detectors due to their good detection efficiency at a >500 nm range, fast response, excellent energy resolution, low operation voltage, and low cost [18–20]. Since the PIN diode and the preamplifier are the more susceptible parts to electronic noise in comparison to the rest of the components in the signal processing unit of the proposed EPD system, an appropriate shielding

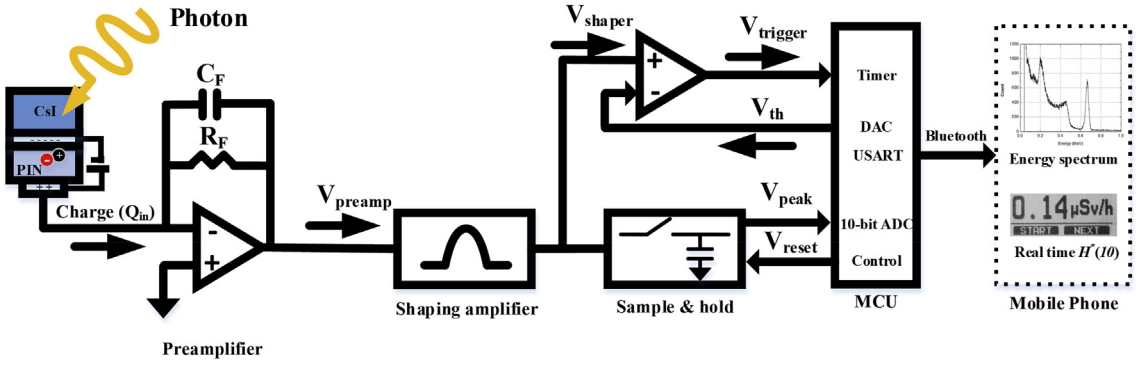

Fig. 1. A simplified schematic of the signal processing unit in the main body of the EPD.

enclosure, e.g., an aluminum shielding case, was adopted. Considering space limitation the minimum efficiency, as well as the fabrication cost, the size of the PIN diode was set as 3 × 3 mm^2 in this study.

As for the choice of scintillator for the EPD, it is necessary to have a high detection efficiency, wide dynamic range, good energy resolution, and a low production cost. More importantly, it must have a good light yield to generate a sufficient amount of charge signals. The CsI(Tl) scintillator is an inexpensive inorganic scintillator that offers a good light yield and an optimal peak emission wavelength. One disadvantage of the CsI(Tl) is that it has a longer decay time in comparison to the other inorganic scintillators [21]. However, EPDs do not require fast signal processing, so this does not influence the detection performance. Therefore, the CsI(Tl) with a size of 3 × 3 × 3 mm^3 was chosen as the scintillator for the proposed EPD system.

To power the amplifiers, the voltage is converted to ±3 V in the main body printed circuit board (PCB) from the external lithium-polymer battery output of 3.7 V. As for the PIN diode, the same 3 V that powers the amplifiers was drawn in order to operate the detector that minimizes the overall power consumption and the complexity of the board design. The generated output pulse from the PIN diode is amplified through the preamplifier and shaping amplifier to achieve a sufficiently large signal for the MCU. The preamplifier is composed of a charge sensitive amplifier (CSA) that converts the charges received from a PIN diode into a voltage, and the shaping amplifier is composed of a CR-RC^5 filter including pole-zero cancellations. At this stage, the pulse width generated from the shaping amplifier is approximately 40 μs. The reason for a relatively long shaping time is because the pulse amplidue of the preamplifier (V_{preamp}) is so small (in order of a few mV) that it takes longer time to amplify V_{preamp}. It should be noted that the shaping time is longer than other known scintillation detectors such as PMTs and SiPMs. Nonetheless, this is not an issue for the designed EPD because the measurement period of the incoming photons does not have to be fast in case of natural radiation detection applications.

The threshold voltage (V_{th}) of the comparator, which is supplied by the digital-to-analog converter (DAC) in the MCU, is set to above the electronic noise level which is equivalent to about 40 keV gamma-ray. When the generated trigger signal ($V_{trigger}$) is supplied to the MCU, the peak signal (V_{peak}) of the shaping amplifier is sent to the MCU through the sample and hold unit. Then, in 10 μs, a reset signal (V_{reset}) is generated by the MCU and sent back to the sample and hold unit to reinitialize the shaping amplifier. The recorded peak signal is then transferred to a 10-bit analog-to-digital converter (ADC) in the MCU, where the ADC signal is finally transmitted to the mobile phone via Bluetooth communication to obtain gamma spectra. This process is repeated until the data acquisition duration reached the time set by the EPD.

2.2. $H^*(10)$ calculation

The relationship between the measured spectrum $M(E)$ and the incident fluence rate $\Phi(E_0)$, where E_0 is the incident photon energy, can be expressed as

$$M(E) = \int_{E_{min}}^{E_{max}} R(E,\ E_0)\phi(E_0)dE_0 \tag{1}$$

where $R(E,E_0)$ is the response function of the EPD system, E_{min} is the minimum gamma-ray energy, and E_{max} is the maximum gamma-ray energy. In this study, E_{min} and E_{max} were set to be 40 keV and 2000 keV, respectively, after considering the electronic noise level and practial limit of gamma-ray energy. Furthermore, the ambient dose equivalent rate $H^*(10)(E_0)$ (in $\mu Sv/h$) generated at a given fluence rate $\Phi(E_0)$ can be described as

$$H^*(10)(E_0) = \phi(E_0)C(E_0) \tag{2}$$

where $C(E_0)$ is the fluence-to-dose conversion factor, which is equal to

$$C(E_0) = \frac{H^*(10)(E_0)}{\phi(E_0)} = \int_{E_{min}}^{E_{max}} R(E,\ E_0)G(E)dE \tag{3}$$

where $G(E)$ is the general spectrum-to-dose conversion function. Thus, in the case of a multi-energy radiation exposure, the ambient dose equivalent rate $H^*(10)$ can be described by combining Eq. (1) and Eq. (3):

$$\begin{aligned} H^*(10) = \sum_i \phi(E_i)C(E_i) &= \sum_i \int_{E_{min}}^{E_{max}} \phi(E_i)R(E,\ E_i)G(E)dE \\ &= \int_{E_{min}}^{E_{max}} \sum_i \phi(E_i)R(E,\ E_i)G(E)dE \\ &= \int_{E_{min}}^{E_{max}} M(E)G(E)dE = \sum_{i=1}^{N} M(E_i)G(E_i) \\ &= \sum_{i=1}^{N} h(E_i) \end{aligned} \tag{4}$$

where the subscript i is the index for the incident gamma-ray photons from a specific source and has a specific energy, and N is the number of channels, or in this case, $N = 1024$. The $h(E)$ is the converted spectra for $H^*(10)$.

According to previous studies related to the $G(E)$ function [8–13], $G(E)$ can be expressed as Eq. (5), and the ambient dose equivalent rate $H^*(10)$ can be represented by Eq. (6):

$$G(E) = \sum_{K=1}^{KMAX} A(K)(\log E)^{K-M-1} \tag{5}$$

where $A(K)$ is a parameter, $KMAX$ is the total number of $A(K)$ terms, and M is a constant.

$$H^*(10) = \sum_{i=1}^{N} M(E_i) \sum_{K=1}^{KMAX} A(K)(\log E_i)^{K-M-1} \tag{6}$$

In the past, several studies have obtained the parameter $A(K)$ by applying the least-square method (LSM) on the measured spectra and dose rates in order to calculate $G(E)$ [10–12].

Despite the fact that the LSM provides optimal estimates of unknown parameters, the method is quite sensitive to the presence of abnormal data points in the provided data set for fitting. As a consequence, one or two irregularities in the input dataset can often skew the LSM output significantly. In contrast, the gradient-descent method (GDM) utilizes the iterative optimization method and therefore, the GDM offers more advantages over the LSM in terms of finding the optimal estimates via iterative process. Therefore, the parameter $A(K)$ was determined by applying the GDM to find the optimal variables owing to the fact that $A(K)$ depends on the value $KMAX$. Furthermore, we generated the function

$G(E)$ by using the gamma spectra and $H^*(10)$ that correspond to 99 mono energies ranging from the minimum energy of 40 keV to the maximum energy of 2000 keV with a step of 20 keV via Monte-Carlo simulation using MCNP6 to accurately fit the $G(E)$ function. This is because ther are not enough number of radioisotope check-sources available to cover the energy region of interest for the designed EPD. Furthermore, the accuracy in fitting the $G(E)$ function increases with increasing number of spectra and $H^*(10)$. In this case, the value M in $G(E)$ was set to zero because the effect of the value M on the dose rate accuracy was known to be negligible in a previous study [12].

The mean squared error (MSE) function for the GDM can be expressed as

$$MSE[A(0),\ A(1),\ \ldots,A(KMAX)] = \frac{1}{L}\sum_{l=1}^{L}\left(H^*(10)_{exp,\ m} - H^*(10)_{known,m}\right)^2 \tag{7}$$

where $H^*(10)_{exp}$ is the expected ambient dose equivalent rate, $H^*(10)_{known}$ is the known ambient dose equivalent rate calculated from the Monte-Carlo simulation, and L is the number of simulated spectra, which is equal to 99. Then the parameter $A(K)$ can be obtained using the GDM to minimize the MSE, i.e.,

$$A(K_{j+1}) = A(K_j) - \alpha\frac{\partial}{\partial A(K_j)}MSE[A(0),\ A(1),\ \ldots,A(KMAX)] \tag{8}$$

where j is the iteration index, α is the learning rate, and the value K ranges from 1 to $KMAX$. In general, the value $KMAX$ is selected from 8 to 14. However, $KMAX$ is selected from 2 to 20 in order to identify the error based on the $KMAX$ value because the accuracy of the dose rate improves when the value of $KMAX$ is greater than 15 [12]. The differentiation term in Eq. (8) can be expressed as Eq. (9) and the differentiation term of Eq. (9), can be expressed as Eq. (10):

$$\frac{\partial}{\partial A(K_j)}MSE[A(0),\ A(1),\ \ldots,A(KMAX)] = \frac{2}{L}\sum_{l=1}^{L}\left(H^*(10)_{exp,\ l} - H^*(10)_{known,l}\right)\frac{\partial D_{exp,l}}{\partial A(K_j)} \tag{9}$$

$$\frac{\partial D_{exp,l}}{\partial A(K_j)} = \sum_{i=1}^{N} M(E_i)\sum_{K=1}^{KMAX}(\log E_i)^{K-1} \tag{10}$$

By using the equations above, the value $A(K)$ was selected where the MSE function had the smallest error. Then, the function $G(E)$ was finally obtained for each corresponding parameter $A(K)$. In addition, the value of $KMAX$ of the $G(E)$ function was chosen for $H^*(10)$ to have a small error value for five radioisotope sources of ^{241}Am, ^{137}Cs, ^{22}Na, ^{54}Mn, and ^{60}Co.

3. Results and discussion

The gamma energy spectra for the radioisotopes of ^{241}Am, ^{137}Cs, ^{22}Na, ^{54}Mn, and ^{60}Co were obtained in the proposed EPD system, as shown in Fig. 2. The spectrum acquisition time was 300 s and the distance between the isotope source and the detector was set to 5 cm. The sensitivity of EPD (in CPS/μSv/h) for $H^*(10)$ for ^{241}Am, ^{137}Cs, ^{22}Na, ^{54}Mn, and ^{60}Co were measured as 922.3, 27.2, 24.4, 20.8, and 12.5, respectively. The result shows that the energy response to ^{137}Cs in the low-energy range is higher than that in the high-energy

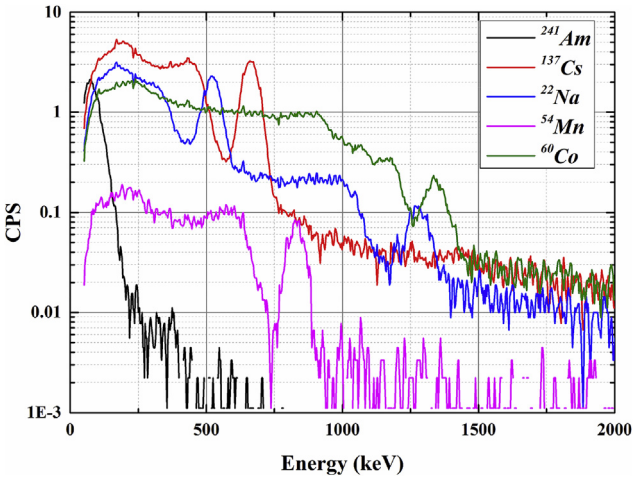

Fig. 2. Gamma spectra measured by EPD on multiple radioisotopes.

range. This implies that the discrepancy between the response function of the detector $R(E,\ E_0)$ and the dose at E_0 is significant in terms of the energy response. Thus, an appropriate $G(E)$ function should be used to solve this problem.

The parameters $A(K)$ in the $G(E)$ function in Eq. (5) were calculated using the GDM for $KMAX$ ranging from *2* to *20*. For all of the $KMAX$ values, the parameters $A(K)$ were initially set to zero, and the learning rate was set as 0.001. To determine the optimal value for $KMAX$, the gamma spectra of ^{241}Am, ^{137}Cs, ^{22}Na, ^{54}Mn, and ^{60}Co were converted to $H^*(10)$ by using each $G(E)$ function. Then the root-mean-square error ($RMSE$) for evaluating the $G(E)$ function for different $KMAX$ values can be obtained through Eq. (11)

$$RMSE = \sqrt{\sum_{t=1}^{T}\left(H^*(10)_{measured,\ t} - H^*(10)_{calculated,\ t}\right)^2 \Big/ T} \tag{11}$$

where $H^*(10)_{measured}$ is the ambient dose equivalent from the measured gamma spectra using each $G(E)$ function, $H^*(10)_{calculated}$ is the ambient dose equivalent calculated from the source strength, and T is the number of radioisotopes, which is equal to five in this case.

Fig. 3 shows the $RMSE$ as a function of $KMAX$ values ranging from 2 to 20. From the figure, we found that the smallest $RMSE$ value, 0.0019, was obtained when the value $KMAX$ was equal to 19. Then the function $G(E)$ for $H^*(10)$ was obtained for $KMAX = 19$, as shown in Fig. 4.

Fig. 4 shows that the value of $G(E)$ varies with respect to the incident photon energy. The role of the $G(E)$ function in the EPD is to equalize the high response at a low energy region and the low response at a high energy region, like a weighting factor. Then the converted spectra for $H^*(10)$, $h(E)$, can be obtained by multiplying

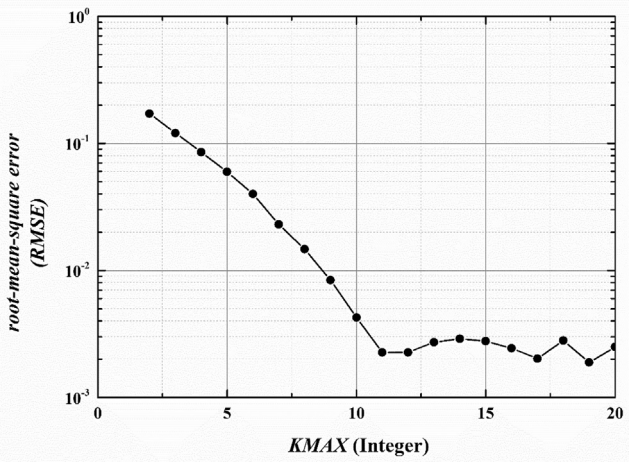

Fig. 3. *RMSE* as a function of *KMAX* ranging from 2 to 20. The minimum *RMSE* of 0.0019 was achieved when *KMAX* was equal to 19.

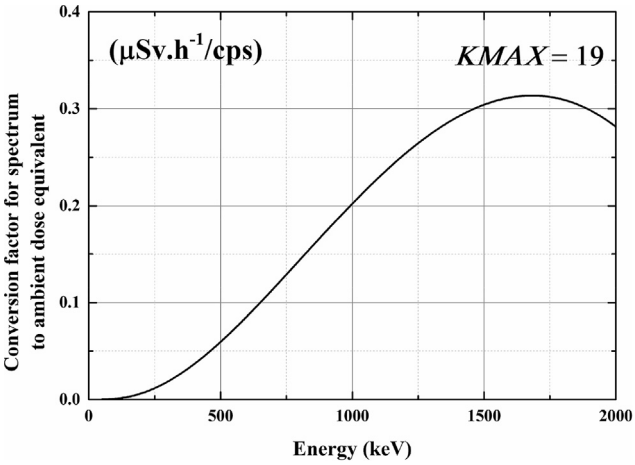

Fig. 4. The $G(E)$ as a function of incident photon energy for $H^*(10)$.

the number of total counts in each channel to the corresponding $G(E)$ values. $H^*(10)$ can also be acquired by summing up all $G(E)$ values. Fig. 5 shows the spectra of ^{137}Cs and ^{60}Co acquired from the EPD and the converted spectra $h(E)$ by using the corresponding $G(E)$ functions.

From Fig. 5, we see that $h(E)$ for ^{60}Co exhibits photo-peaks corresponding to 1.17 MeV and 1.33 MeV,which are more intuitively distinguished than the existing spectrum due to the high $G(E)$ value in the high energy region. In addition, we see that the partial absorption such as Compton scattering in the low energy region is reduced while the full energy peak is more distinguished.

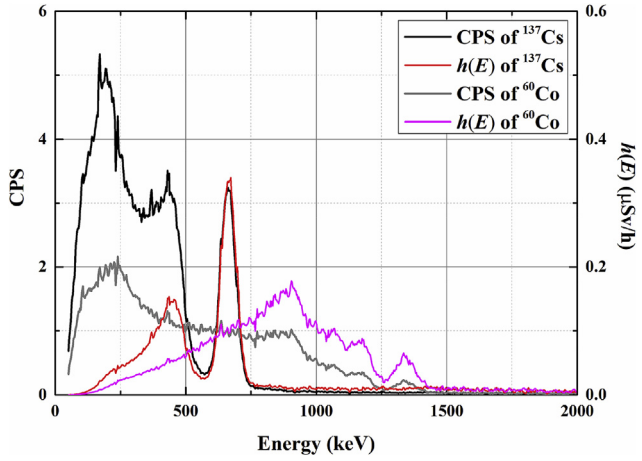

Fig. 5. The measured spectra for ^{137}Cs and ^{60}Co and the converted spectra, $h(E)$, for $H^*(10)$.

Thus, it is advantageous to utilize a small-sized PIN diode in EPDs not only for measuring the $H^*(10)$, but also for identifying radioisotope types. Table 1 shows the dose measurements acquired from the designed EPD for each source with the $G(E)$ function obtained by the LSM and GDM. We can easily see that the LSM shows a large relative difference of −13.88% at the low energy region of ^{241}Am. In contrast, the difference is much smaller with the GDM, i.e., ±2.89% for all energies and therefore, this clearly demonstrates that the $G(E)$ function obtained by is GDM more accurate than that of the LSM.

Fig. 6 shows the energy response normalized to 662 keV of ^{137}Cs of $H^*(10)$ for five radioisotopes using Eq (12).

$$\text{Energy response} = \frac{\frac{CPS_E}{H^*(10)_E}}{\frac{CPS_{662keV}}{H^*(10)_{662keV}}} \tag{12}$$

where $\frac{CPS_E}{H^*(10)_E}$ is the sensitivity at an energy E (in CPS/μSv/h), $\frac{CPS_{662keV}}{H^*(10)_{662keV}}$ is the sensitivity at 662 keV of ^{137}Cs (in CPS/μSv/h).

As for the counting method that is typically used in conventional EPDs, the energy response was high in the low energy region while the response was low in the high energy region. However, the energy response obtained through the converted spectra $h(E)$ using the $G(E)$ function lie in between the values of 0.97 and 1, which is equivalent to ± 3% for the photon energy ranging from 59.5 to 1250 keV. Thus, this clearly demonstrates that the obtained $G(E)$ function can correct the energy response of the designed EPD with a higher accuracy in comparison to that of the conventional counting method.

Since the designed EPD operates in a pulse mode, the maximum dose rate can be determined according to the pulse period in the system:

Table 1
$G(E)$ used to measure $H^*(10)$.

Isotope	Mean energy (keV)	$H^*(10)_{calculated}$ (μSv/h)	$H^*(10)_{measured\_LSM}$ (μSv/h)	LSM relative difference (%)	$H^*(10)_{measured\_GDM}$ (μSv/h)	GDM relative difference (%)
^{241}Am	59.5	0.0504	0.0434	−13.88	0.0502	−0.4
^{137}Cs	662	24.28	24.28	0	24.294	0.06
^{22}Na	784	15.017	14.781	−1.574	14.986	−0.21
^{54}Mn	835	1.316	1.289	−2.02	1.279	−2.89
^{60}Co	1250	35.729	35.584	−0.41	35.735	0.02

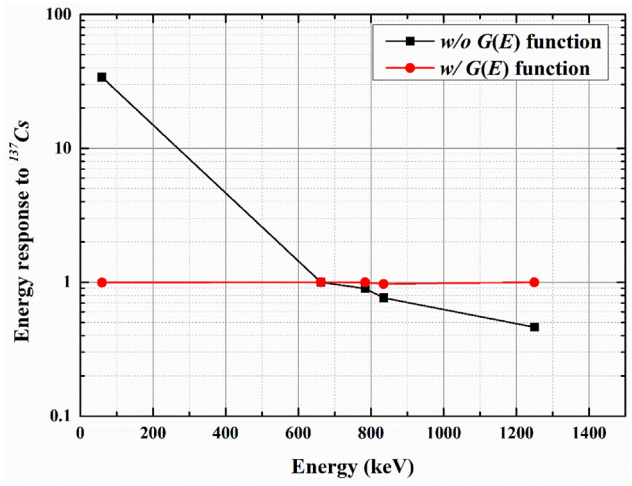

Fig. 6. The energy response to ^{137}Cs of $H^*(10)$ for the designed EPD.

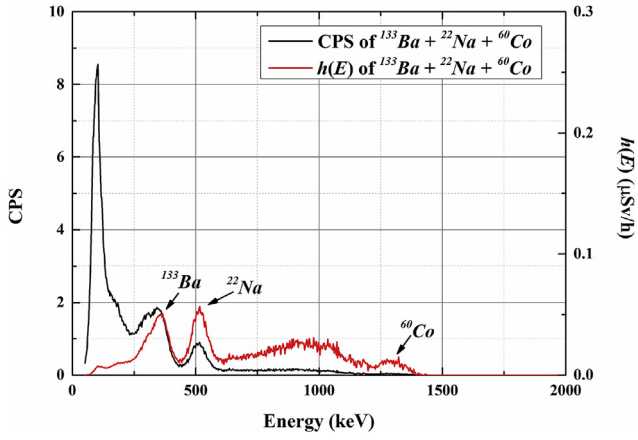

Fig. 7. The gamma spectra of mixed multiple sources of ^{133}Ba, ^{22}Na and ^{60}Co obtained by Monte-Carlo simulation and the converted spectra, $h(E)$, for $H^*(10)$.

$$H^*(10)_{max}[Sv/h] = \phi(E_{max}) \times C(E_{max}) = \frac{CPS_{max}}{\varepsilon(E_{max})} \times C(E_{max}) \times 3600sec \quad (13)$$

where $\phi(E_{max})$ is the fluence at the measured maximum energy E_{max}, $C(E_{max})$ is the fluence-to-$H^*(10)$ conversion factor at E_{max}, CPS_{max} is the maximum measurable counts per second and $\varepsilon(E_{max})$ is the detection efficiency at E_{max}. The maximum energy that the designed EPD system can detect is equal to 2 MeV and CPS_{max} is equal to 25,000 counts per second due to its long shaping time. Furthermore, the $\varepsilon(2MeV)$ was obtained by a MCNP simulation which is equal to 6.15% and $C(2MeV)$ was obtained according to ICRP74. Given that $C(2MeV)$ at the detector size of 0.09 cm^2 is equal to 95.6 pSv, the maximum detectable dose rate of the designed EPD system is approximately equals to 140 mSv/h.

Furthermore, it is necessary to verify the accuracy of $H^*(10)$ conversion in the case of multiple sources. Since available gamma check sources were limited, different types and activity ratios of radioisotopes were generated via the MCNP6 simulation. Fig. 7 shows an example of the gamma spectra and the converted spectra $h(E)$ obtained for a mixed source of ^{133}Ba, ^{22}Na, and ^{60}Co with 51%, 29%, and 20% activity ratios, respectively. The radioisotopes were well identified by photo-peaks from the obtained $h(E)$. Table 2 shows the calculate $H^*(10)$ based on the $G(E)$ function for each spectrum based on the simulation. From the result, we can clearly see that the relative differences for all cases fall within ±5.56%, even for the multiple radioisotope case.

4. Conclusion

In this manuscript, we demonstrated a gamma spectroscopy based conversion method for $H^*(10)$ in an EPD with a 3 × 3 mm^2 PIN diode coupled to a 3 × 3 × 3 mm^3 CsI(Tl) scintillator. The function $G(E)$ was obtained by applying the GDM to convert the acquired spectrum to its corresponding $H^*(10)$ directly. Under the identical condition, the gamma spectra for ^{241}Am, ^{137}Cs, ^{22}Na, ^{54}Mn, and ^{60}Co were obtained by using the designed EPD. Then, the measured gamma spectra were converted to $H^*(10)$ using the $G(E)$ function by the GDM. From the results, we found that the relative differences of all five isotopes fall within the range of ±2.89% and therefore, we demonstrated that the $G(E)$ function obtained by the GDM holds more accurate results than that of the $G(E)$ function obtained by the conventional LSM. In addition, the energy response of $H^*(10)$ fell within ±3% for photon energies ranging from 59.5 to 1250 keV. Furthermore, the gamma spectra and $H^*(10)$ were obtained by mixing various ratios of several radioisotopes via Monte-Carlo simulation to verify the accuracy of the $H^*(10)$ conversion in the case of a multiple radioisotope case. By comparing the $H^*(10)$ calculated from the $G(E)$ function with the simulated $H^*(10)$, we found that the relative difference was in the range of ±5.56%. Furthermore, the proposed method for acquiring the $G(E)$ function through the GDM is not only applicable for scintillation detection with PMTs or SiPMs, but also for direct detectors such as CZT and CdTe. For future work, we plan to compare and analyze the performance of the $G(E)$ function based on the GDM by applying the fabricated EPD system with respect to other commercial EPDs.

Table 2
$G(E)$ used to measure $H^*(10)$ for multiple sources.

Isotopes	$H^*(10)_{calculated}$ (μSv/h)	$H^*(10)_{measured}$ (μSv/h)	Relative difference (%)
^{133}Ba (51%) + ^{22}Na (29%) + ^{60}Co (20%)	8.823	8.852	0.33
^{133}Ba (30%) + ^{131}I (21%) + ^{60}Co (21%) + ^{192}Ir (17%) + ^{54}Mn (11%)	7.821	8.079	3.19
^{54}Mn (54%) + ^{60}Co (28%) + ^{22}Na (18%)	11.116	10.536	−5.5
^{54}Mn (42%) + ^{22}Na (27%) + ^{60}Co (24%) + ^{137}Cs (7%)	10.885	10.312	−5.56
^{54}Mn (40%) + ^{131}I (32%) + ^{133}Ba (21%) + ^{137}Cs (7%)	6.634	6.398	−3.69
^{22}Na (36%) + ^{137}Cs (32%) + ^{60}Co (28%) + ^{192}Ir (4%)	10.934	10.511	−4.02

Acknowledgments

This research was supported by the KUSTAR-KAIST Institute, KAIST, Korea and the Center for Integrated Smart Sensors funded by the Ministry of Science and ICT as Global Frontier Project (CISS-2016M3A6A6929965).

Appendix A. Supplementary data

Supplementary data to this article can be found online at https://doi.org/10.1016/j.net.2019.06.017.

References

[1] International Comission on Radiation Units and Measurements, Quantities and Units in Radiaiton Protectrion Dosimetry, 1996.
[2] P. Buzhan, A. Karakash, Teverovskiy Yu, Silicon photomultiplier and Csi(Tl) scintillator in application to portable H*(10) dosimeter, Nucl. Instrum. Methods Phys. Res. Sect. A Accel. Spectrom. Detect. Assoc. Equip. 912 (2018) 245–247.
[3] R. Casanovas, E. Prieto, M. Salvado, Calculation of the ambient dose equivalent H*(10) from gamma-ray spectra obtained with scintillation detectors, Appl. Radiat. Isot. 118 (2016) 154–159.
[4] A. Camp, A. Vargas, Ambient dose estimation H*(10) from Labr3(Ce) spectra, Radiat. Protect. Dosim. 160 (4) (2014) 264–268.
[5] C.Y. Yi, et al., Measurement of ambient dose equivalent using a Nai(Tl) scintillation detector, Radiat. Protect. Dosim. 74 (4) (1997) 273–278.
[6] P. Kessler, et al., Novel spectrometers for environmental dose rate monitoring, J. Environ. Radioact. 187 (2018) 115–121.
[7] International Commission on Radiological Protection, Conversion Coefficients for Use in Radiological Protection against External Radiation, vol. 74, ICRP Publication, 1996.
[8] S. Tsuda, et al., Characteristics and verification of a Car-borne survey system for dose rates in air: kurama-ii, J. Environ. Radioact. 139 (2015) 260–265.
[9] S. Tsuda, K. Saito, Spectrum-dose conversion operator of Nai(Tl) and Csi(Tl) scintillation detectors for air dose rate measurement in contaminated environments, J. Environ. Radioact. 166 (Pt 3) (2017) 419–426.
[10] P. Huang, Measurement of air kerma rate and ambient dose equivalent rate using the G(E) function with hemispherical cdznte detector, Nucl. Sci. Tech. 29 (3) (2018) 35.
[11] S. Moriuchi, I. Miyanaga, A spectrometric method for measurement of low-level gamma exposure dose, Health Phys. 12 (1966) 541–551.
[12] H. Terada, et al., Spectrum-to-Exposure rate conversion function of a Ge(Li) in-situ environmental gamma-ray spectrometer, IEEE Trans. Nucl. Sci. 24 (1) (1977) 647–651.
[13] Masahiro Tsutsumi, Yoshihiko Tanimura, $LaCl_3$(Ce) scintillation detector applications for environmental gamma-ray measurements of low to high dose rates, Nucl. Instrum. Methods Phys. Res. Sect. A Accel. Spectrom. Detect. Assoc. Equip. 557 (2) (2006) 554–560.
[14] D.B. Pelowitz, et al., MCNP6 User's Manual, version 1.0, Report No. LA-CP-13-00634, Rev. 0, Los Alamos National Laboratory, 2013.
[15] P. Buzhan, et al., Silicon photomultiplier and its possible applications, Nucl. Instrum. Methods Phys. Res. Sect. A Accel. Spectrom. Detect. Assoc. Equip. 504 (1–3) (2003) 48–52.
[16] B. Dolgoshein, et al., Status report on silicon photomultiplier development and its applications, Nucl. Instrum. Methods Phys. Res. Sect. A Accel. Spectrom. Detect. Assoc. Equip. 563 (2) (2006) 368–376.
[17] P. Buzhan, et al., An advanced study of silicon photomultiplier, in: Proceedings of the Seventh International Conference on Advance Technology & Particle Physics, 2002, pp. 717–728.
[18] Daisuke Totsuka, et al., Performance test of Si pin photodiode line scanner for thermal neutron detection, Nucl. Instrum. Methods Phys. Res. Sect. A Accel. Spectrom. Detect. Assoc. Equip. 659 (1) (2011) 399–402.
[19] B.E. Patt, et al., High resolution CsI(Tl)/Si-PIN detector development for breast imaging, IEEE Trans. Nucl. Sci. 45 (1998) 2126–2131.
[20] D. Clément, et al., Development of a 3D position sensitive scintillation detector using neural networks, IEEE Nucl. Sci. Symp. Conf. Rec. (1998) 1448–1452.
[21] F. Knoll, Glenn, Radiation Detection and Measurement, John wiley & Sons, 2010.